Journal of Zhejiang University SCIENCE A
ISSN 1009-3095 (Print); ISSN 1862-1775 (Online)
www.zju.edu.cn/jzus; www.springerlink.com
E-mail: jzus@zju.edu.cn

Research and development of fringe projection-based methods in 3D shape reconstruction*

WU Lu-shen[1], PENG Qing-jin‡[2]

([1]*Department of Mechanical and Electronic Engineering, Nanchang University, Nanchang 330029, China*)

([2]*Department of Mechanical and Industrial Engineering, University of Manitoba, R3T 5V6, Canada*)

E-mail: wulushen@hotmail.com; Pengq@cc.umanitcba.ca

Received Oct. 20, 2005; revision accepted Jan. 16, 2006

Abstract: This paper discusses current research and development of fringe projection-based techniques. A system based on Fourier transform profilometry (FTP) is proposed for three-dimensional (3D) shape recovery. The system improves the method of phase unwrapping to gain accurate 3D shapes of objects. The method uses a region-growing algorithm for the path prediction guided by the quality map to increase the recovering accuracy and provides a fast and simple tool for 3D shape recovery. The shape measurement and data recovery are integrated to offer a new method of 3D modelling. Examples are presented to verify the feasibility of the proposed method.

Key words: 3D modelling, Fringe projection, Quality map, 3D measurement, Reverse engineering
doi:10.1631/jzus.2006.A1026 **Document code:** A **CLC number:** TP391.4

INTRODUCTION

Geometric modelling is essential processing in computer-aided engineering (CAE) systems. Usually, the modelling of three-dimensional (3D) objects is embedded in a computer-aided design (CAD) system, which may take a huge amount of time to build entire models for CAE application. One option is the use of techniques of reverse engineering (RE) to build models from existing objects. Coordinate measuring machines (CMMs) are traditional RE tools used in the manufacturing industry and provide high measuring accuracy and stability, but the disadvantages are the contact measurement and slow point-by-point measuring processing. Besides CMMs, optical technology has been significantly applied in the 3D shape capturing and reconstruction. The optical method provides no-contact data acquisition processing to facilitate rapid capturing of data on existing objects. Examples of the application include image-based RE for measuring the shape of sheet metal parts (Yan and De, 2003); the vision sensor for free-form surfaces reconstruction (Lai *et al*., 2001); combining stereo-vision and shape-from-shading recovery for obtaining reliable shape (Bae and Benhabib, 2003); and scanning the surface of an unknown object through the utilization of optical range sensors (Martins *et al*., 2003).

This paper uses the fringe projection technique to search for an accurate solution to recover 3D shapes of objects. Simple system structure and cost-effective technique are objectives of the research. The following parts of the paper discuss related research, techniques developed, system implementation and application examples.

RELATED RESEARCH

Optical measurement techniques based on fringe

‡ Corresponding author

* Project (No. 59965003) supported by the National Natural Science Foundation of China

or grating analysis have been widely used for acquiring 3D object shapes. Fringe or grating analysis utilizes non-interfering lighting and image processing technology to gain data on 3D shapes. The method projects a sinusoidal fringe pattern on an object surface. The height change of the surface is transformed into the phase distribution of the deformed fringe when the fringe is projected on the object. Demodulation can then be used to abstract the low-frequency component by using filtering processing (Srinivasan *et al*., 1995; Tang and Hung, 1990). The fringe phase method requires a simple structure of the lighting system. Rapid calculation and automation can be used in the data capturing and processing. The following techniques have been developed for fringe projection-based 3D shape recovery (Xu and Wang, 1998; Yamaguchi *et al*., 2001).

1. Phase-shift grating projection (PGP): this method has features of high accuracy, and effectiveness against noise of the image background, can provide high space resolution, and can process complicated bordering problems. However, this method relies on a highly accurate hardware system. Accurate phase-shift facility has to be available in the system and requires that the phase shifts more than twice, and so, multiple sample captures are needed. Vibration of the object under test may be a problem adversely affecting the processing speed.

2. Sinusoidal spatial phase detection (SPD): the deformed fringe is multiplied by sin and cosine functions that have the same angular frequency as that of the fringes in order to shift the frequency spectrum. Independent information on the first-grade spectrum can be obtained using a lowpass in the space field. This method can get results rapidly at relatively high accuracy if there is suitable lowpass available.

3. Cosine exchange method: it transforms the deformed fringe that is shifted one fourth period using cosine. A lowpass is applied to abstract information on the base frequency. The phase information contained in the surface height can then be obtained by arc-cosine transform. This method uses the transform of a real number field, and requires less computing time than that of Fourier transform profilometry (FTP), and so, is about four times faster than FTP. However, this method requires one phase shift and two images in the processing, which limits its applications. Other similar methods have been suggested for processing fringe intensity directly, including the phase-demodulation method and the digital image processing method (Wu and Yu, 1993).

4. Fourier transform profilometry (FTP) (Takeda *et al*., 1982; Takeda and Mutoh, 1983): it uses Fourier transform for the deformed fringe and reference fringe, and shifts the first-grade spectrum into the original spectrum in the frequency field. A lowpass is then used on the phase frequency field to filter the direct and other high-frequency components on the image background with the remaining first-grade spectrum then computed by conjugate-multiplication, with its result being calculated by logarithm. Finally, the component of the solution's imaginary numbers will be the phase value resulted from the surface profile change. The frequency spectrum of the phase image generated by Fourier transform enables convenient and easy processing. FTP has features of high-accuracy measurement and wide applications. The disadvantage is the high computing cost. Current computers have enough capacity to meet this requirement.

Comparison of current fringe projection methods for the 3D shape recovery showed that:

(1) There is no perfect method without limitations. The solution of a 3D shape recovery system depends on the performance of both hardware and software. A high-accuracy hardware of the image capturing system brings about a better solution of the shape recovery, but the equipment cost will be increased significantly. This work is aimed at searching for a cost-effective solution that mainly uses an effective algorithm to improve the performance of the system.

(2) FTP is simple, with the processing being done in the frequency field, so that the generated result in the lowpass filtering is better than that in space field. Design of lowpass in the frequency field is relatively easy. The frequency spectrum of the processed image by Fourier transform can be displayed graphically which makes the spectrum analysis and the lowpass design easy.

(3) Phase-shift grating projection and cosine exchange methods require accurate and complex phase shift equipment. At least two deformed fringe images have to be collected to ensure high accuracy of the processing. Comparatively, only one deformed phase image is required when FTP method is used.

(4) FTP can remove high-frequency noise and the slowly-changing grey-scale noise in the image background, so that the requirement for image capturing environments is low, which is useful in practical applications.

(5) FTP has relatively mature 2D transform algorithms compared to other methods that can only process 1D transform. So if there are available a well designed 2D lowpass filter and a high performance computer that can provide the high speed and memory required, a feasible 3D shape capturing system can be achieved. So in this research FTP was selected as the explored technique for recovering 3D shapes of existing objects.

3D SHAPE RECOVERY BASED ON FRINGE PROJECTION

Fringe projection uses a sinusoidal fringe pattern projected on the surface of an object. The deformed pattern on the object is captured by a CCD camera, with the image being then sent to the computer for FTP processing. The height distribution of the object can be obtained by decomposing the profile function of the object. Fringe projection techniques are the basis of the method. Information on the object profile is usually encoded into deformed fringe pattern. Thus, by observing the fringe pattern from a different direction of the fringe projection, the surface profile of the object can be measured. The optical system used in this research is shown in Fig.1. A sinusoidal fringe pattern is projected at a certain angle onto the object and a CCD camera acquires the image of the deformed fringe on the object. If the phase difference of fringes on the reference plane and on the object surface could be measured, the surface profile of the object can be determined accurately.

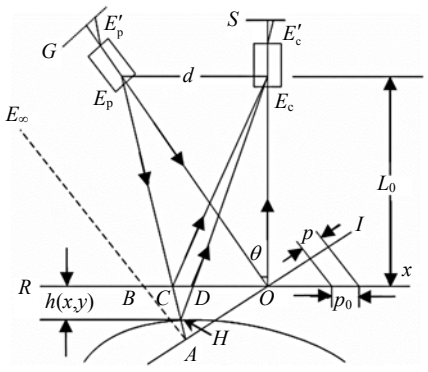

Fig.1 Structure of the optical system

Fig.1 shows the structure of the image capturing system with the intersection optical axes. Where, E'_p, E_p are the projection directions of the fringe pattern, E'_c, E_c are the directions of camera axis, and they intersect at O on plate R. E_p and E_c have the same distances to R, and the distances equal L_0. $h(x, y)$ is the height of the object surface measured from R. When a virtual sinusoidal fringe pattern generated by the computer is projected on the reference plate R, an image of the pattern can be captured by the CCD camera. The image is originally undeformed pattern which can be expressed as:

$$g_0(x,y)=\sum_{n=-\infty}^{\infty}A_n\exp\{\mathrm{j}[2\pi nf_0x+n\varphi_0(x,y)]\}, \quad (1)$$

where x axis is directed normal to the fringe, y axis is parallel to the direction of the fringe. f_0 is the base frequency of the pattern image $\varphi(x,y)$, and f_0 represents the modulated initial phase. When the object exists, the deformed fringe image can be obtained by the CCD camera and then sent to the computer for processing:

$$g(x,y)=r(x,y)\sum_{n=-\infty}^{\infty}A_n\exp\{\mathrm{j}[2\pi nf_0x+n\varphi(x,y)]\}, \quad (2)$$

where, $r(x,y)$ is the distribution of reflection rates of the object surface, $\varphi(x,y)$ is the modulated phase resulted from the height change of the object surface. Using 1D Fourier transform for Eq.(2), the result is the frequency spectrum. The zero frequency shows the density of lighting distribution in the object background, and the base frequency gives the required phase information for the height recovery.

A band-pass filter can be used to filter one component of the base frequency, and then inverse Fourier transform is used on the result. The distribution of the lighting density can be obtained as:

$$G(x,y)=A_1r(x,y)\exp\{\mathrm{j}[2\pi f_0x+\varphi(x,y)]\}. \quad (3)$$

Using the same filtering operation for Eq.(1), the

distribution of the lighting density in the reference surface R can be obtained as:

$$G_0(x,y) = A_1 \exp\{\mathrm{j}[2\pi f_0 x + \varphi_0(x,y)]\}. \quad (4)$$

From the geometric relation in Fig.1:

$$\Delta\varphi(x,y) = \varphi(x,y) - \varphi_0(x,y), \quad (5)$$

$\Delta\varphi(x,y)$ contains the height information of the object, but the phase is wrapped. The continuous phase distribution can be calculated using an unwrapping algorithm. Finally, the height data of the object can be obtained as:

$$h(x,y) = \frac{\Delta\varphi(x,y) L_0 p_0}{2\pi d + \Delta\varphi(x,y) p_0}, \quad (6)$$

where, d is the distance between projector and camera, and L_0 is the distance between reference plate R and projector or camera.

A detailed processing of the height recovery is shown in Fig.2. The image of the deformed fringes is pre-processed to reduce noises generated in the image capturing before Fourier transform is used on the image. The first-grade distribution of main frequency f_0, and band width b can then be determined. After that, spectra are filtered, and inverse Fourier transform is used to get the main value of the phase, with the same process being applied on the reference phase image subtracted from the phase value of the deformed image to get the difference of phase $\Delta\varphi(x,y)$. Finally, the height distribution of the object is obtained using Eq.(6).

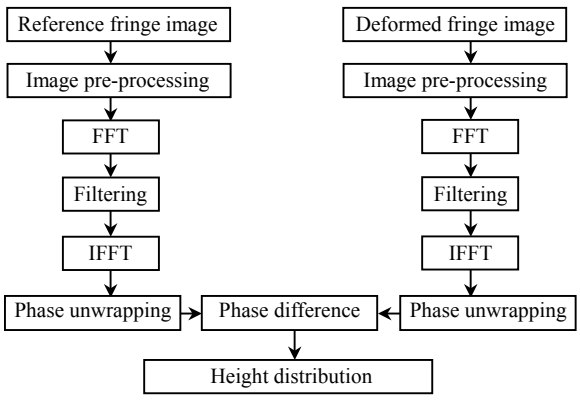

Fig.2 Flow chart of Fourier transform profilometry

Three processes are important in reducing the error and improving the accuracy in the object recovery. Image denoising and filtering are required to get the spectra, and phase unwrapping is required to get the phase difference as shown in Fig.2. Among them, the phase unwrapping is a key process for acquiring the height distribution of the object.

Phase unwrapping recovers the phase value wrapped in the range of $-\pi$~$+\pi$. An earlier technique used in phase unwrapping adopted linear scanning methods, using the phase value of neighboring points. But these methods can easily generate errors in the wrapping direction of the phase, called "stretch-line" (Itoh, 1982).

Later in 1987, the cellular automata method (Ghiglia *et al*., 1987) was proposed to improve the processing accuracy. The method first isolates the noise points, and then uses iteration calculation along rows and columns of the phase image to obtain the whole value of the phase field. The advantage of this method is that the phase value around the noise point can be adjusted automatically for denoising. But it depends on the identification of the isolated noise point and the discontinuous phase values resulted from the small number of samples used. Therefore, this method can only tell the position of the noise, not the accurate location of the discontinuous phase values. Errors are often generated. The iteration calculation is also time-consuming.

The noise-immune cut method was suggested by Goldstein *et al*.(1988). This method had been successfully used in the phase unwrapping of 2D interference images captured by satellite radar. Huang also proposed a similar algorithm (Huang and Lai, 2002) whose basic concept is to first search for the noise locations, then match pairs using the sign of the noise points, and then set the discontinuous lines in the wrapped phase image.

The phase unwrapping is then processed around these lines to eliminate the effects of the noise and discontinuous lines. The key processing is to pair noise points with opposite signs, which uses the minimal distance rule. Later, Cusack *et al*.(1995) used the stable marriage pair method to match the noise points with opposite signs.

The phase unwrapping by region was proposed by Stetson *et al*.(1997). This method separates the phase image into areas that do not contain discon-

tinuous lines of phase values, unwrapping phase for each region, and comparing values at the border of regions to find any jump of phase values. The rule to decide the region is to keep the phase difference in a limited range. This method does not refer to the position of the noise and the normal jump of phase values. The threshold value is unadjusted.

Shortcomings of these methods include long computational time, requirement of human interaction to check if the pairs are correct, and the limited discontinuous lines required (Judge and Bryanston-cross, 1994; Takeda and Abe, 1996). Different problems exist in current phase unwrapping algorithms (Dougherty and Selkow, 2004; Magnus *et al*., 2004). The threshold has to be set very small so that there are no discontinuous lines in each region, which results in too many regions to adjust (Pearson, 2005). The authors used a new method for phase unwrapping. The method first removes the isolated noise point, and then unwraps the phase gradually using a region-growing algorithm guided by the quality map. It is effective in reducing errors in phase unwrapping, and eliminating the "stretch-line".

IMPROVED ALGORITHM FOR PHASE UNWRAPPING

Basis of phase unwrapping

In the mathematical description of traditional phase unwrapping methods (Gierloff, 1987), the phase value from the arc-tangent calculation was considered as the result of the wrapping calculation for the measured phase:

$$W_1[\phi(n)] = \phi_{\mathrm{pv}}(n),\ n = 0, 1, 2, \ldots, N \tag{7}$$

where, $\phi_{\mathrm{pv}}(n)$ is the main value, subscript 1 indicates different wrapping calculations.

$$W_1[\phi(n)] = \phi(n) + 2k_1(n),\ n=0, 1, 2, \ldots, N \tag{8}$$

where, $k_1(n)$ is an integer series.

$$-\pi \le W_1[\phi(n)] \le \pi. \tag{9}$$

Let

$$\Delta\phi(n) = \phi(n) - \phi(n-1),\ n=0, 1, 2, \ldots N \tag{10}$$

The difference of phase main values is:

$$\Delta W_1[\phi(n)] = \Delta\phi(n) + 2k_1(n). \tag{11}$$

The main values can be calculated once again by the wrapping algorithm:

$$W_2\{\Delta W_1[\phi(n)]\} = \Delta\phi(n) + 2\pi[\Delta k_1(n) + k_2(n)]. \tag{12}$$

It is the wrapping difference generated by phase wrapping. As values calculated by the wrapping algorithm locate in $[-\pi,+\pi]$, therefore,

$$-\pi \le \Delta\phi(n) \le \pi, \tag{13}$$

and the second item of the right hand side of Eq.(12):

$$2\pi[\Delta k_1(n) + k_2(n)] = 0.$$

Therefore,

$$\Delta\phi(n) = W_2\{\Delta W_1[\phi(n)]\}, \tag{14}$$

and

$$\phi(m) = \phi(0) + \sum_{n=1}^{m} W_2\{\Delta W_1[\phi(n)]\}. \tag{15}$$

Eq.(15) shows that phase can be unwrapped by the sum of differences of the wrapping main values. It also shows the error distribution along unwrapping directions, the causative reason for the "stretch-line" generated in the real phase map. When Eq.(13) is not satisfied because of poor demodulated points, the noise, or dust from inadequate sampling, it will adversely affect the unwrapping path. Therefore, the key for correct unwrapping is to identify and eliminate points that do not satisfy Eq.(13) by stopping the error extension.

Identifying and eliminating isolated noise points

According to the sampling rule, the number of sampling points has to be greater than two pixels in one period. Therefore, the phase difference of adjacent pixels must be in the range of $-\pi$~$+\pi$. For the easy description, a jump value is defined as follows for any two adjacent pixels:

$$d_i = \begin{cases} -1, & \phi_i - \phi_{i-1} < -\pi, \\ 0, & -\pi \le \phi_i - \phi_{i-1} \le \pi, \\ 1, & \phi_i - \phi_{i-1} > \pi, \end{cases} \tag{16}$$

or

$$d_i = n \cdot \mathrm{int}\left(\frac{\phi_i - \phi_{i-1}}{2\pi}\right), \tag{17}$$

where, $n\cdot\mathrm{int}(x)$ indicates that d_i takes the nearest integer of the value in the bracket, specially, $n\cdot\mathrm{int}(\pm 0.5)=0$.

The noise points can be located by the following procedure:

(1) Taking randomly adjacent four pixels as a unit in the map, wrapping phases of these four pixels are $\phi(i,j)$, $\phi(i,j+1)$, $\phi(i+1,j)$, $\phi(i+1,j+1)$, respectively, as shown in Fig.3a.

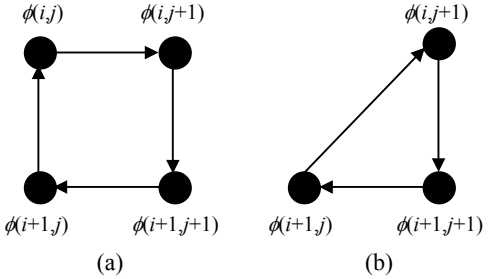

Fig.3 Search of isolated noise points. (a) Searching for four adjacent pixels; (b) Searching for three adjacent pixels

(2) Starting from $\phi(i,j)$, along the clockwise direction shown in Fig.3a, the jump-change value of two adjacent points can be summed using Eq.(17):

$$\begin{aligned} d = \sum_{i=1}^{4} d_i = {} & n \cdot \mathrm{int}\left(\frac{\phi(i,j+1)-\phi(i,j)}{2\pi}\right) \\ & + n \cdot \mathrm{int}\left(\frac{\phi(i+1,j+1)-\phi(i,j+1)}{2\pi}\right) \\ & + n \cdot \mathrm{int}\left(\frac{\phi(i+1,j)-\phi(i+1,j+1)}{2\pi}\right) \\ & + n \cdot \mathrm{int}\left(\frac{\phi(i,j)-\phi(i+1,j)}{2\pi}\right). \end{aligned} \tag{18}$$

If $d=0$, there is no noise point in this unit, then go to next unit. If $d\neq 0$, there are noise points in this unit.

Similarly, Eq.(17) can be used to calculate the sum of jump-changed value of adjacent pixels for three points in sequence. The calculation of the sum of jump-changed values of adjacent pixels along the direction shown in Fig.3b is as follows:

$$\begin{aligned} d = \sum_{i=1}^{3} d_i = {} & n \cdot \mathrm{int}\left(\frac{\phi(i+1,j+1)-\phi(i,j+1)}{2\pi}\right) \\ & + n \cdot \mathrm{int}\left(\frac{\phi(i+1,j)-\phi(i+1,j+1)}{2\pi}\right) \\ & + n \cdot \mathrm{int}\left(\frac{\phi(i,j+1)-\phi(i+1,j)}{2\pi}\right), \end{aligned} \tag{19}$$

if $d=0$, $\phi(i,j)$ is not the noise point. Otherwise, the three points have to be searched in sequence.

(3) Processing other points in the phase map using Steps (1) and (2) will result in a phase map with identified noise points. These isolated noise points can be removed using filtering technologies.

Quality map

Quality map is an array used for the distribution of information quality in displaying the phase map. It is abstracted from the phase map except extremum points, which can be used to improve the quality of phase unwrapping. The quality map may have different definitions and may provide different information when different optical measuring systems are used. The earliest quality map was defined by the second-order partial derivative. The phase unwrapping was for the pixel where the value of its second-order partial derivative is less than a pre-defined threshold. A statistical method is introduced in this research to decide the quality map from the phase derivation variance calculated in the area masked by $k\times k$ from the pixel location (m, n):

$$v_{m,n} = \frac{\sqrt{\sum(\Delta^x_{i,j} - \overline{\Delta}^x_{m,n})^2}}{k^2} + \frac{\sqrt{\sum(\Delta^x_{i,j} - \overline{\Delta}^y_{i,j})^2}}{k^2}, \tag{20}$$

$$\Delta^x_{i,j} = \{\phi_{i+1,j} - \phi_{i,j}\},\ \Delta^y_{i,j} = \{\phi_{i,j+1} - \phi_{i,j}\},$$

where, $\Delta^x_{i,j}$ and $\Delta^y_{i,j}$ are the partial derivatives of the phase in the range $[-\pi,+\pi]$. $\overline{\Delta}^x_{m,n}$ and $\overline{\Delta}^y_{m,n}$ are the average of partial derivatives in a $k\times k$ window. It is clear from the definition that a greater change of the derivative will result in worse quality of the map. The quality is best when the change of the derivative is zero. Therefore, the quality map can be used to decide the sequence of phase unwrapping. The process starts from the best quality pixel.

Region-growing algorithm

The growing track was fixed in traditional region-growing algorithms, which cannot unwrap the complex phase map effectively. Different directions are considered in this research for complex phase maps using the region-growing algorithm based on the path prediction proposed. The algorithm improves the accuracy of the phase unwrapping by reducing the error distribution, which includes the following processing:

(1) Starting from a point or a region, called the seed point or seed region that is the smoothest part of the region, the unwrapping is extended to the outside along the predicted path.

(2) Unwrapping of each pixel is based on the linear prediction of its surrounding pixels that have been unwrapped. The prediction allows that the phase difference of two adjacent pixels is greater than π.

(3) Using as many pixels that have been unwrapped in the unwrapping processing to reduce the error that may be generated from one single prediction direction.

The unwrapping process is considered as a state engine. The state of each unwrapping consists of one or many continued unwrapping pixel regions. The neighbour of each pixel forms the link for the next unwrapping iteration. This pixel is called a growing pixel. Therefore, the unwrapping result does not depend on the integrated solution but the individual pixel in the neighbouring region. The phase difference between two adjacent pixels can be allowed greater than π in the region where there are large height variations in the fringe image. Examples have shown that the algorithm can tell the mixed phase value correctly in complex cases.

Region-growing algorithm for the path prediction guided by the quality map

The proposed algorithm unwraps the pixel guided by the quality map. The region-growing moves along the direction of the best quality. Combining the denoising processing, the procedure can be described as follows:

(1) Identifying and removing isolated noise points using the method described in Section 4.2.

(2) Calculating the quality map of the entire image.

(3) Selecting the best part from the quality map as the breeding region to start the unwrapping. Linear unwrapping is firstly used.

(4) Starting from the unwrapped area, showing all possible growing pixels.

(5) Selecting the best point as a current growing point from these possible pixels, unwrapping the pixel using the method discussed in Section 4.4.

(6) Go to (4) until all pixels are unwrapped following the growing directions.

Multi-seeds growing simultaneously can be used in phase unwrapping for the large-sized phase map. Next section discusses the hardware configurations and the error analysis of the optical system in the image capturing.

ERROR ANALYSIS OF THE IMAGE CAPTURING SYSTEM

The hardware configuration is one of the factors affecting the accuracy of shape recovery. Inaccurate parameters, L_0, d, p_0, used in the optical system shown in Fig.1, will bring errors to the shape measurement.

Effect of p_0

Considering the effect of p_0 in Eq.(6),

$$h(x,y)=\frac{\Delta\varphi(x,y)L_0p_0}{2\pi d+\Delta\varphi(x,y)p_0},$$

the partial derivative of p_0 is as follows:

$$\frac{\partial h(x,y)}{\partial p_0}=\frac{2\pi dL_0\Delta\phi(x,y)}{[2\pi d+\Delta\phi(x,y)p_0]^2},$$

or

$$\Delta h(x,y)=\frac{2\pi dL_0\Delta\varphi(x,y)}{[2\pi d+\Delta\varphi(x,y)p_0]^2}\Delta p_0, \tag{21}$$

where, $\Delta h=h-h_e$, $\Delta p_0=p_0-p_{0e}$, h_e and p_{0e} are measured values, h and p_0 are ideal values. In the optical system, L_0 or d is much greater than p_0, and $p_0\Delta\phi(x,y)<<2\pi d$, therefore,

$$\Delta h(x,y)=\frac{L_0\Delta\phi(x,y)}{2\pi d}\Delta p_0. \tag{22}$$

Eq.(22) shows that the height error is proportional to the ratio of L_0/d. Eq.(6) can be rewritten as:

$$\Delta\phi(x,y)=\frac{2\pi d h(x,y)}{p_0 L_0 - p_0 h(x,y)}. \quad (23)$$

Combining Eqs.(21) and (23) yields the following equation:

$$\Delta h(x,y)=\frac{-h^2(x,y)+L_0 h(x,y)}{p_0 L_0}\Delta p_0. \quad (24)$$

Therefore, the height error is a function of height h, period p_0 and distance L_0. The error is proportional to the height of the point recovered. If the system meets $h(x,y)<<L_0$, Eq.(24) can be simplified as:

$$\Delta h(x,y)=\frac{h(x,y)}{p_0}\Delta p_0. \quad (25)$$

It clearly shows that the height error is proportional to height h, and the relative error of period, Δp_0.

Effect of *d*

Considering the effect of d in Eq.(6), the partial derivative of d is as follows:

$$\frac{\partial h(x,y)}{\partial d}=\frac{-2\pi L_0 p_0 \Delta\phi(x,y)}{[2\pi d+\Delta\phi(x,y)p_0]^2}, \quad (26)$$

or

$$\Delta h(x,y)=\frac{-2\pi L_0 p_0 \Delta\phi(x,y)}{[2\pi d+\Delta\phi(x,y)p_0]^2}\Delta d, \quad (27)$$

where $\Delta h=h-h_e$, $\Delta d=d-d_e$, h_e and d_e are measured values, h and d are the ideal values. In practice, L_0 and d are much greater than p_0, $p_0\Delta\phi(x,y)<<2\pi d$, therefore, Eq.(27) can be written as:

$$\Delta h(x,y)=-\frac{L}{2\pi d^2}p_0\Delta\phi(x,y). \quad (28)$$

Combining Eqs.(27) and (28) yields:

$$\Delta h(x,y)=\frac{h^2(x,y)-L_0 h(x,y)}{dL_0}\Delta d. \quad (29)$$

If $h(x,y)<<L_0$ holds, Eq.(29) can be simplified to:

$$\Delta h(x,y)=\frac{h(x,y)}{d}\Delta d, \quad (30)$$

which shows that the height error is proportional to h and Δd.

Effect of L_0

Considering the effect of L_0 in Eq.(6), its partial derivative of L_0 is as follows:

$$\frac{\partial h(x,y)}{\partial L_0}=\frac{p_0\Delta\phi(x,y)}{2\pi d+p_0\Delta\phi(x,y)}, \quad (31)$$

similar to the effect of p_0 in Section 5.1,

$$\Delta h(x,y)=\frac{p_0\Delta\phi(x,y)}{2\pi d+p_0\Delta\phi(x,y)}\Delta L_0, \quad (32)$$

where, $\Delta h=h-h_e$, $\Delta L_0=L_0-L_{0e}$, h_e and L_{0e} are measured values, h and L_0 are ideal values. In practice, L_0 and d are much greater than p_0, therefore, Eq.(32) can be written as:

$$\Delta h(x,y)=\frac{p_0\Delta\phi(x,y)}{2\pi d}\Delta L_0. \quad (33)$$

Combining Eqs.(32) and (33), and considering $h(x,y)<<L_0$, yields

$$\Delta h(x,y)=\frac{h(x,y)}{L_0}\Delta L_0, \quad (34)$$

which shows that the height error is proportional to h and ΔL_0.

Experiment and analysis

A spherical object was used to test the system configuration and error analysis. The captured image resolution was 512×512 pixels. System parameters, L_0=70 cm, d=14 cm, and p_0=8 lines/mm were used. The deformed fringe image on the spherical object is shown in Fig.4. The recovered profile of the sphere is shown in Fig.5.

In order to get the error distributions of the above data, the initial system parameters of L_0, d, and p_0 were assumed as the ideal values. Then L_0, d, and p_0 were changed to observe errors generated in the shape recovery processing. Fig.6 is the height error distribution when L_0, d, and p_0 are increased 5%, respectively.

It can be observed from Fig.6 that L_0 will change

the surface convex, d will shape the surface concave, and p_0 will turn the surface twist upward when the parameters are increased 5% from the ideal values. When the parameters are decreased by 5% from the ideal values, L_0, d, and p_0 will change oppositely.

APPLICATION EXAMPLES

A concave mold shown in Fig.7 was selected to test the proposed method. The hardware system was constructed as shown in Fig.1. The system configuration parameters were measured. The shape recovery procedures are shown in Fig.8. The sinusoidal fringe pattern used is shown in Fig.8a, which is a computer generated virtual pattern projected to the reference surface to get a reference unformed image. The deformed image is shown in Fig.8b, which was captured after the mold was located in the reference surface. Fig.8c is the wrapped phase graph. The unwrapped phase graph is shown in Fig.8d. Using Eq.(6), the height data can be recovered as shown in Fig.8e. Fig.8f is the reconstructed mold.

The part of a human body plaster model was used to evaluate the accuracy obtained using the proposed method and using the traditional algorithm. Fig.9 shows the comparison results. Figs.9e and 9f are the results generated by the traditional method. Figs.9g and 9h are the results using the proposed method. It is obvious that there is no "stretch-line" in the results of the proposed method. The recovery accuracy is improved. Therefore, phase noise points and discontinuous lines can be reduced using the FTP phase unwrapping algorithm.

Fig.10 shows another application to recover the shape of a human body model. A deformed gratings map of the model is shown in Fig.10a. Fig.10b is the wrapped phase map. Fig.10c is unwrapped phase map generated by the proposed method. The recovered model shape is shown in Fig.10d.

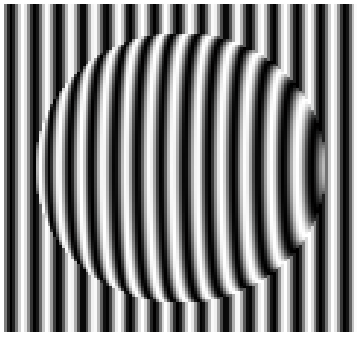

Fig.4 Deformed grating image on the spherical object

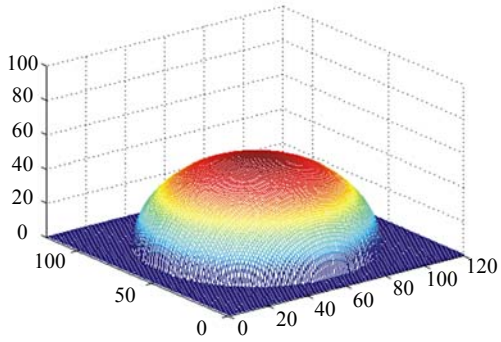

Fig.5 Recovered profile of the sphere

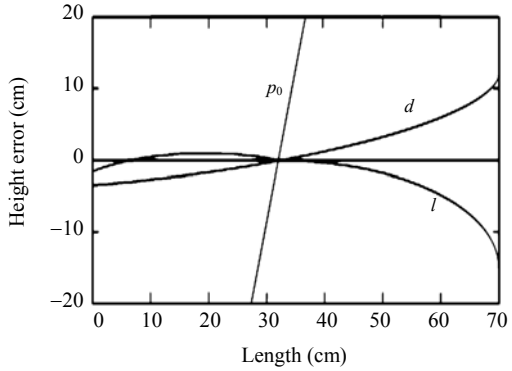

Fig.6 Height error when increasing L_0, d, and p_0 5%, respectively

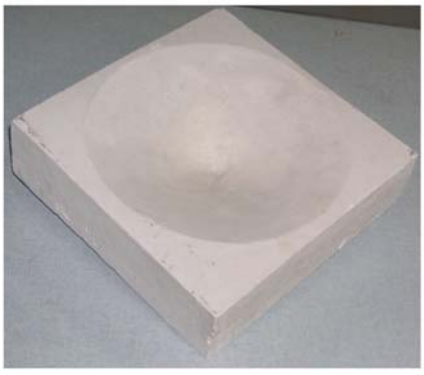

Fig.7 Concave mold

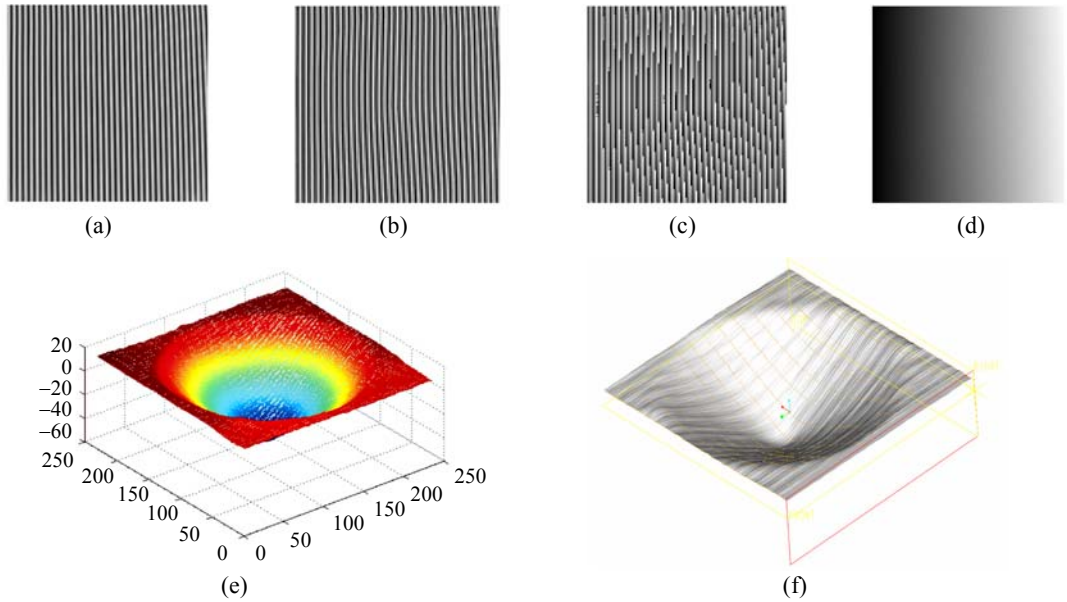

Fig.8 Recovery procedure of the concave model. (a) Sinusoidal fringe pattern; (b) Deformed pattern; (c) Wrapped phase graph; (d) Unwrapped phase graph; (e) Recovered 3D data; (f) Reconstructed concave mold

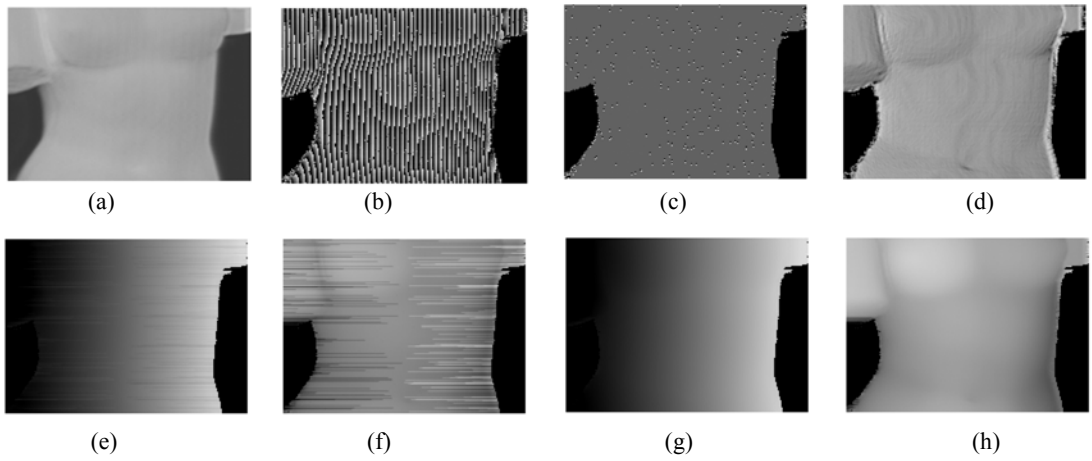

Fig.9 Example of human body plaster model. (a) Model picture; (b) Wrapped phase graph; (c) Isolated noise map; (d) Quality map; (e) Unwrapped phase using traditional algorithm; (f) Retrieval phase map from (e); (g) Wrapped phase using the proposed algorithm; (h) Retrieved phase map from (g)

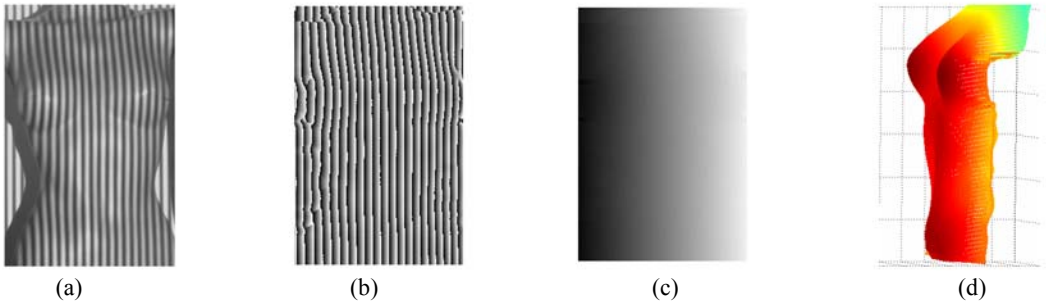

Fig.10 Recovery of a human body model. (a) Deformed gratings map of the model; (b) Wrapped phase map; (c) Unwrapped phase map; (d) Recovered model shape

CONCLUSION AND FURTHER WORK

This paper describes a fringe projection-based method for 3D shape reconstruction. A region-growing algorithm is proposed to improve the accuracy of the phase unwrapping of FTP-based techniques. Hardware factors affecting the system accuracy and a quantitative accuracy analysis are presented. Accuracy comparison with other methods is only based on a visual examination of the smoothness of recovered surfaces. There is need to introduce a criterion of quantitative accuracy of the "stretch-line". The surface roughness may be used and the related measurement method is required to find the quantitative accuracy of the proposed method.

The system was tested on an off-line processing procedure. The time for convergence of the algorithm has not been considered as a critical factor. It will be essential for real-time application, which will be a part of further work. The proposed method is very useful for small and medium size objects, but not for large-sized objects, such as buildings and manufacturing workshops, and may not capture the full scene of the model construction. Other alternatives, such as triangles-based profilometry techniques can be used to abstract key points of a large object, while using the proposed method to obtain detailed information on the object. Further research will be aimed towards these solutions.

References

Bae, K.Y., Benhabib, B., 2003. A hybrid scheme incorporating stereo-matching and shape-from-shading for spatial object recognition. *Proceedings of the Institution of Mechanical Engineers, Part B: Journal of Engineering Manufacture*, **217**(11):1533-1542. [doi:10.1243/095440503771909917]

Cusack, R., Huntley, J.M., Goldrein, H.T., 1995. Improved noise-immune phase unwrapping algorithm. *Applied Optics*, **35**(5):781-789.

Dougherty, D.J., Selkow, S.M., 2004. The certification of properties of stable marriage. *Information Processing Letters*, **92**(6):275-277. [doi:10.1016/j.ipl.2004.09.006]

Ghiglia, D.C., Mastin, G.A., Romero, L.A., 1987. Cellular-automata method for phase unwrapping. *Journal of Optical Society of American*, **4**(1):267-280.

Gierloff, J.J., 1987. Phase unwrapping by regions. *Optical Engineering*, **818**:2-9.

Goldstein, R.M., Zebker, H.A., Werner, C.L., 1988. Satellite radar interferometry: two-dimensional phase unwrapping. *Radio Science*, **23**(4):713-720.

Huang, M.J., Lai, C., 2002. Phase unwrapping based on a parallel noise-immune algorithm. *Optics and Laser Technology*, **34**(6):457-464. [doi:10.1016/S0030-3992(02)00042-7]

Itoh, K., 1982. Analysis of the phase unwrapping algorithm. *Applied Optics*, **21**(14):2470-2486.

Judge, T.R., Bryanstoncross, P.J., 1994. A review of phase unwrapping techniques in fringe analysis. *Optics and Lasers in Engineering*, **21**(4):199-239. [doi:10.1016/0143-8166(94)90073-6]

Lai, X.M., Li, Z.Q., Huang, T., Zeng, Z.P., 2001. A study of a reverse engineering system based on vision sensor for free-form surfaces. *Computers and Industrial Engineering*, **40**(3):215-227. [doi:10.1016/S0360-8352(01)00022-5]

Magnus, M.H., Kazuo, I., Shuichi, M., Hiroki, Y., 2004. Randomized approximation of the stable marriage problem. *Theoretical Computer Science*, **325**(3):439-465. [doi:10.1016/j.tcs.2004.02.045]

Martins, F.A.R., Garcia-Bermejo, J.G., Zalama, E., Peran, J.R., 2003. An optimized strategy for automatic optical scanning of objects in reverse engineering. *Proceedings of the Institution of Mechanical Engineers, Part B: Journal of Engineering Manufacture*, **217**(8):1167-1171.

Pearson, D., 2005. A polynomial-time algorithm for the change-making problem. *Operations Research Letters*, **33**(3):231-234. [doi:10.1016/j.orl.2004.06.001]

Srinivasan, V., Liu, H.C., Halioua, M., 1995. Automated phase-measuring profilometry: a phase mapping approach. *Applied Optics*, **24**(2):185-187.

Stetson, K.A., Wahid, J., Gauthier, P., 1997. Noise-immune phase unwrapping by use of calculated wrap regions. *Applied Optics*, **36**(20):4830-4838.

Takeda, M., Mutoh, K., 1983. Fourier transform profilometry for the automatic measurement of 3D object shapes. *Applied Optics*, **22**(24):3977-3982.

Takeda, M., Abe, T., 1996. Phase unwrapping by a maximum cross-amplitude spanning tree algorithm: A comparative study. *Optical Engineering*, **35**(8):2345-2351. [doi:10.1117/1.600810]

Takeda, M., Ina, H., Koboyashi, S., 1982. Fourier-transform method of fringe-pattern analysis for computer-based topography and interferometry. *Journal of Optical Society of America*, **72**(1):156-160.

Tang, S., Hung, Y., 1990. Fast profilometer for the automatic measurement of 3-D object shapes. *Applied Optics*, **29**(20):3012-3018.

Wu, P.F., Yu, F.H., 1993. Analysis technique for the measurement of a three-dimensional object shape. *Applied Optics*, **32**(5):737-742.

Xu, J., Wang, Y., 1998. 2D Fourier Transform and Automatic Reference Grating Image Method for Optical Measurement of 3D Surface Shapes. SPIE's International Symposium on Optical Science, Engineering and Instrumentation. San Diego.

Yamaguchi, L., Ohta, S., Kato, J., 2001. Surface contouring by phase-shifting digital holography. *Optics and Lasers in Engineering*, **36**(5):417-428. [doi:10.1016/S0143-8166(01)00069-0]

Yan, J., De, S.L., 2003. Reverse Engineering of Sheet Metal Parts Using Machine Vision. Proc. the ASME Design Engineering Technical Conference, p.1085-1095.